particles

MDPI

Conference Report

Short-Lived Resonances as Probes of the Medium Produced in Heavy-Ion Collisions

Victor Riabov [1,2]

[1] NRC «Kurchatov Institute»-PNPI, 1, mkr. Orlova roshcha, 188300 Gatchina, Russia; riabov_vg@pnpi.nrcki.ru
[2] National Research Nuclear University MEPhI (Moscow Engineering Physics Institute), Kashirskoe Highway 31, 115409 Moscow, Russia

Abstract: Hadronic resonances play an important role in the study of the physics of heavy-ion collisions. In these proceedings, we discuss how the resonances can probe the reaction dynamics, the strangeness production and the properties of the hadronic phase in heavy-ion collisions at center-of-mass energies of $\sqrt{s_{NN}}$ = 4–11 GeV. The resonance properties predicted by the general-purpose event generators are found to be very sensitive to the properties and space-time evolution of the medium produced in heavy-ion collisions.

Keywords: heavy-ion collisions; short-lived hadronic resonances; hadronic phase; strangeness

1. Introduction

Hadronic resonances are excited hadronic states with relatively short lifetimes. The resonances are copiously produced in hadronic and heavy-ion collisions and are widely accessible for experimental measurements in the dominant hadronic decay channels. Even if charged hadron identification is not possible at low momenta below several hundreds of MeV/c, the momentum range of measurements for resonances can span to zero momenta due to the difference between the masses of parent and daughter particles effectively increasing the daughter particle momenta. At higher momenta, where identification of hadrons with different techniques becomes problematic, the particle multiplicities and hence the combinatorial background become reasonably low to allow for the extraction of the resonance peaks in the accumulated invariant mass distributions. All these make measurements of resonances experimentally possible in a wide range of transverse momentum (p_{T}) even in the high multiplicity environment realized in central heavy-ion collisions. For the measurements, the experimental setup should provide a high-efficiency of track reconstruction in a wide acceptance with a momentum resolution of ~1% and identification of the charged hadrons in the final state.

The interest in the measurement of resonances is motivated by their high sensitivity to different aspects of the heavy-ion collisions. The resonances, which differ by mass and quark content, provide insights into the mechanisms that drive the multiplicity-dependent enhancement of strangeness production and can be used to study Parton energy loss and anomalous baryon-to-meson ratios at intermediate transverse momentum. Due to their short lifetimes, the hadronic resonances are sensitive to the rescattering and regeneration processes occurring between the chemical and the kinetic freeze-out in heavy-ion collisions. Measurements of resonance yields and their ratios to the long-lived particles are used to study the properties and lifetime of the late hadronic phase. The resonance yields and line-shapes measured in the hadronic and leptonic decay channels probe the particle production mechanisms and the collision dynamics.

The most advanced measurements for resonances in heavy-ion collisions are from the experiments at SPS, RHIC and the LHC [1–8]. These experiments developed the basic techniques for the reconstruction of resonances and showed in what areas the resonances contribute to their physical programs. In these proceedings, we effectively expand the

Citation: Riabov, V. Short-Lived Resonances as Probes of the Medium Produced in Heavy-Ion Collisions. *Particles* **2021**, *4*, 1–10. https://dx.doi.org/10.3390/particles4010001

Received: 3 December 2020
Accepted: 21 December 2020
Published: 25 December 2020

previous experience of the resonance studies and the inferred physics messages to the case of lower collision energies expected at the NICA collider, which is now under construction at JINR in Dubna, Russia [9].

2. The Framework for the Study of Resonance Properties

NICA collider is expected to start its regular operation only a few years from now. While we are waiting for data to come, we can use different general-purpose event generators to estimate the resonance properties. The most often measured hadronic resonances are listed in Table 1 along with their basic properties such as mass, width, quark content, lifetime and the most promising decay channels for the reconstruction [10]. For the event generators we used the UrQMD v.3.4 [11], PHSD [12], AMPT [13], EPOS 1.99 and EPOS LHC [14] and DCMQGSM + SMM [15].

Table 1. Properties of the short-lived hadronic resonances [10].

Particle	Mass (MeV/c^2)	Width (MeV/c^2)	Quarks	Decay	BR (%)
$\rho(770)^0$	770	150	$\frac{u\bar{u}+d\bar{d}}{\sqrt{2}}$	$\pi^+\pi^-$	100
$K^*(892)^\pm$	892	50.3	$u\bar{s}$, $\bar{u}s$	$\pi^\pm K^0_s$	33.3
$K^*(892)^0$	896	47.3	$d\bar{s}$	$\pi^\pm K^\pm$	66.7
$\phi(1020)$	1019	4.3	$s\bar{s}$	K^+K^-	48.9
$\Sigma(1385)^+$	1383	36	uus	$\pi^+\Lambda$	87
$\Sigma(1385)^-$	1387	39.4	dds	$\pi^-\Lambda$	87
$\Lambda(1520)$	1520	15.7	uds	K^-p	22.5
$\Xi(1530)^0$	1532	9.1	uss	$\pi^+\Xi^-$	66.7

The study of the resonance production with the UrQMD, PHSD and AMPT event generators is not a trivial task. As short-lived particles, the resonances are decayed by the generators, and only the final state particles are available in the output files. In this case, the resonance yields can be estimated by accumulating the invariant mass distributions for different combinations of daughter particles, integrating the peaks from decays of the resonances in the distributions and correcting them for the branching ratios. The whole procedure resembles what is done for the resonance reconstruction in real data analyses only with ideal particle identification and 100% detector efficiency. Some of the event generators (for example, UrQMD [11]) have an option to disable the decays of a given particle. Then the particle appears in the output files surviving to the final state. However, it was found that the resonance yields estimated from the invariant mass distributions or taken from the output files differ, as demonstrated in Figure 1. The figure shows the ratios of the yields estimated for $\rho(770)^0$ and $\phi(1020)$ mesons with the UrQMD in Au + Au collisions at $\sqrt{s_{NN}}$ = 11 GeV using the two different approaches. One can see that the $\rho(770)^0$ yields are affected by a factor of 3–5, and the $\phi(1020)$ yields are affected by a factor of 2 in different p_T intervals. The difference can be explained by the rescattering and regeneration processes taking place in the hadronic phase. One of the daughter particles can rescatter with the surrounding hadrons or even be absorbed in the inelastic process. As a result of the decorrelation of daughter particles or the loss of one of the daughters, the original resonance cannot be reconstructed. Such processes result in the reduced reconstructed yields of the resonances. However, there is a competing process when the hadrons recombine in new resonances, which increases the resonance yields. The cumulative effect of rescattering and regeneration depends on the lifetime of the resonance, type of daughter particles and properties of the hadronic phase, such as its lifetime, density, etc. For most of the cases, the rescattering prevails over the regeneration, and the total effect is a suppression of the measured resonance yields in high-multiplicity collisions. In case when the resonance yields are estimated from the invariant mass distributions of daughter particles, both effects are taken into account. When resonance decays are disabled, the rescattering effect is canceled out (there are no daughters), while the regeneration effect is still effective and

increases the resonance yield. This explains the ratios shown in Figure 1. All resonance yields presented in this study were obtained using the invariant mass method.

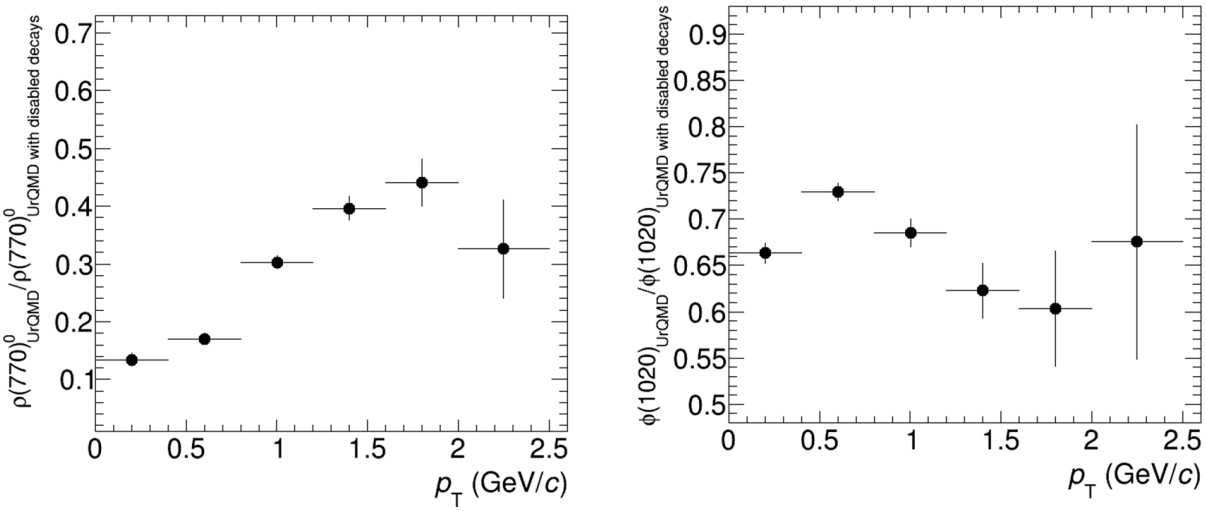

(**a**) (**b**)

Figure 1. Ratios of p_T-differential yields estimated for $\rho(770)^0$ (**a**) and $\phi(1020)$ (**b**) mesons using the two different approaches described in the text. The results are obtained using the UrQMD [11] event generator in Au + Au collisions at $\sqrt{s_{NN}}$ = 11 GeV.

3. p_T-Differential Production Spectra

The comparison of p_T-differential production spectra predicted by different event generators for $\rho(770)^0$, K*$(892)^0$, $\phi(1020)$ and $\Lambda(1520)$ resonances in Au + Au collisions at $\sqrt{s_{NN}}$ = 9 GeV is shown in Figure 2. The ratios of the spectra to the predictions of the UrQMD event generator are shown in Figure 3 on a linear scale. The particle yields were extracted from the invariant mass distributions of daughter particles in the decay modes listed in Table 1. A few million events were simulated for each collision system and event generator to reduce the statistical uncertainties. The systematic uncertainties for the extracted yields are driven by uncertainties in the shape of the combinatorial background. The uncertainties constitute ~10% for all p_T intervals and are not shown in the plots for better visibility. In the ratios shown in Figure 3, the systematic uncertainties of the numerator and denominator partly cancel out. The corresponding uncertainty was estimated to be equal to ~5%.

One can see that the event generators predict quite different yields for the resonances. Similar discrepancies for the predicted resonance yields are also observed at lower and higher collision energies in the range $\sqrt{s_{NN}}$ = 4–11 GeV. For $\rho(770)^0$, K*(892) and $\phi(1020)$ mesons, the EPOS 1.99 and EPOS LHC event generators [14] predict the largest yields, while the UrQMD [11] and the DCMQGSM+SMM [15] predict the lowest yields. The $\Lambda(1520)$ is produced only in the UrQMD and EPOS event generators with rather different p_T-dependencies of the yields.

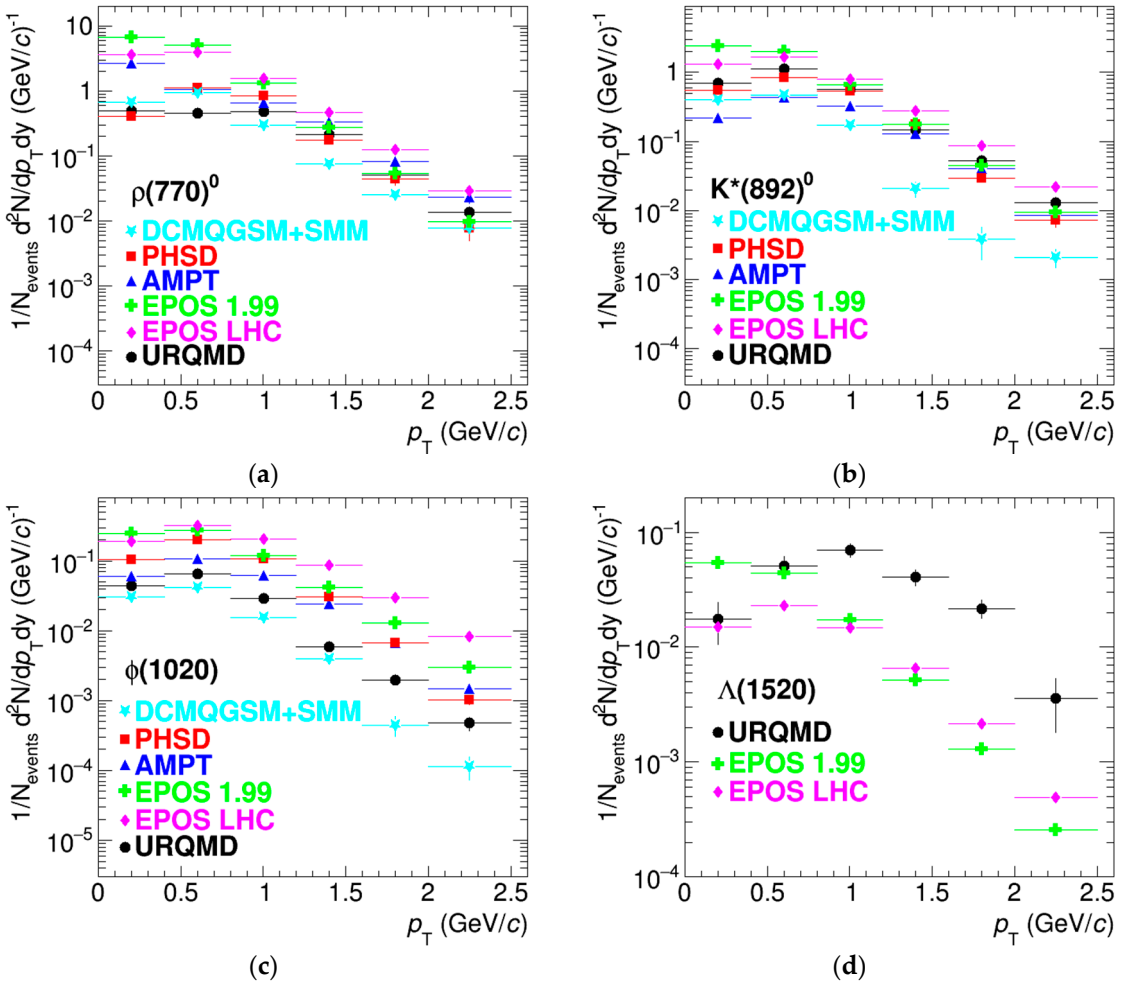

Figure 2. p_T-differential production spectra estimated for $\rho(770)^0$ (**a**), $K^*(892)^0$ (**b**), $\phi(1020)$ (**c**) and $\Lambda(1520)$ (**d**) resonances in Au + Au collisions at $\sqrt{s_{NN}}$ = 9 GeV using different event generators referenced in the text. Statistical uncertainties are shown with error bars. Systematic uncertainties constitute ~10% and are not shown for better visibility.

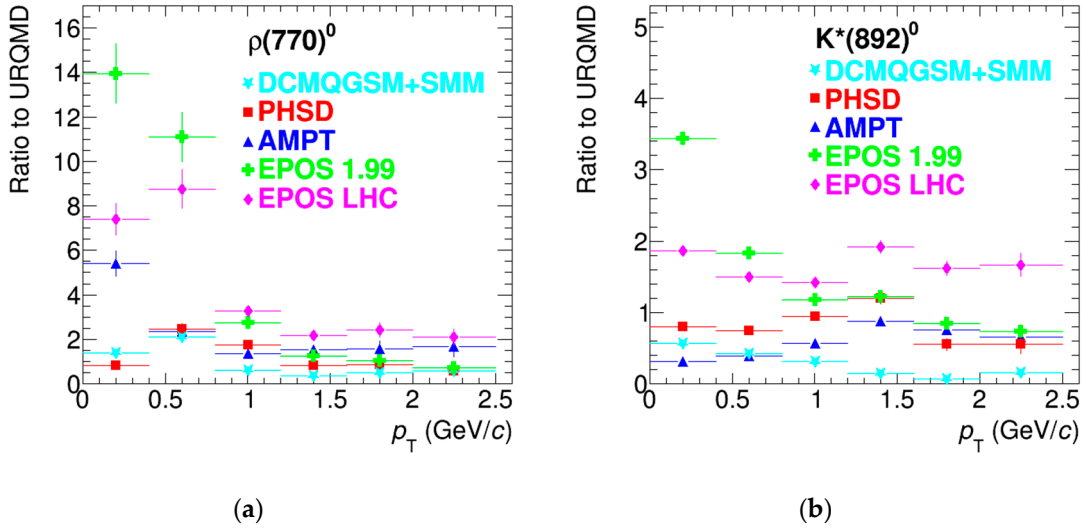

Figure 3. *Cont.*

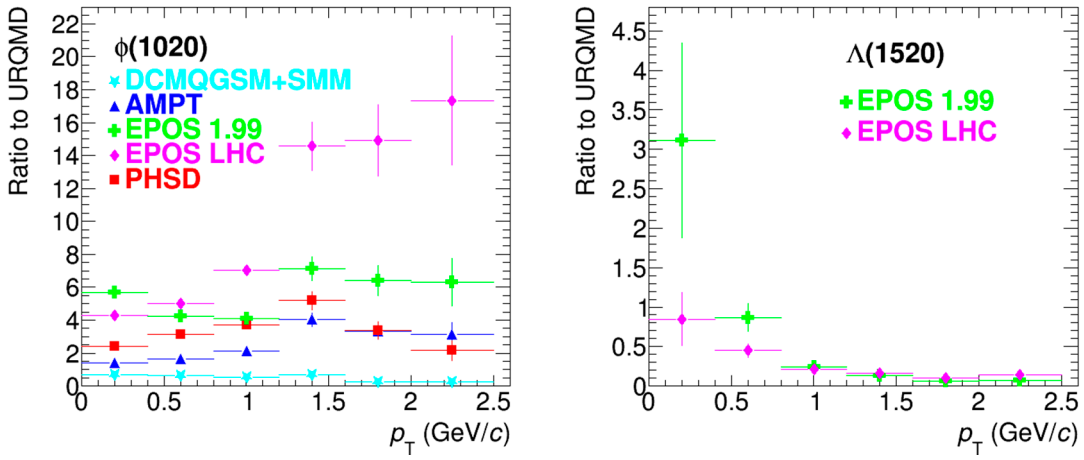

Figure 3. Ratios of p_T-differential yields predicted for $\rho(770)^0$ (**a**), $K^*(892)^0$ (**b**), $\phi(1020)$ (c) and $\Lambda(1520)$ (**d**) resonances by different event generators in Au + Au collisions at $\sqrt{s_{NN}}$ = 9 GeV to the UrQMD [11] predictions. Statistical uncertainties are shown with error bars. Systematic uncertainties are ~5% and are not shown for better visibility.

4. Particle Ratios

As shown in the previous section, the predicted p_T-differential yields of resonances show a strong model dependence. However, common patterns in the production of resonances can be seen from the comparison of the particle ratios in which most of the differences cancel out.

All considered event generators predict enhanced production of particles containing strange quarks in central Au + Au collisions at $\sqrt{s_{NN}}$ = 4–11 GeV. The enhancement is observed as a function of the final state charged-particle multiplicity as for ground-state hadrons as for resonances. Examples of the p/π, K^0_s/π, $\phi(1020)/\pi$, Λ/π, Ξ/π and Ω/π ratios predicted by different event generators in Au + Au collisions at $\sqrt{s_{NN}}$ = 7.7 GeV are shown in Figure 4. One can see that the ratios increase with multiplicity, and the enhancement is more prominent for particles containing a larger number of s-quarks. The maximum enhancement is observed for Ω baryon, which consists of three strange quarks. The $\phi(1020)$ meson, which consists of $s\bar{s}$ pair and has hidden strangeness plays a key role in the study of mechanisms that drive the enhanced production of strangeness.

At LHC energies, the canonical suppression in thermal models, which explain the observed enhancement by suppression of strangeness production at small multiplicities, could quantitatively reproduce the observed multiplicity dependence of strangeness production in pp, p-Pb and Pb-Pb collisions [16,17]. Only the $\phi(1020)$ meson is falling out of the pattern predicted for nonstrange particles, showing an enhancement similar to that for particles with open strangeness. At NICA energies, the event generators predict the enhanced production of $\phi(1020)$ meson in central Au + Au collisions at $\sqrt{s_{NN}}$ = 11 GeV and modest-to-no enhancement at lower collision energies. Eventually, a comparison of model predictions to real data measurements will help to differentiate the different strangeness production mechanisms. The strange resonances and the $\phi(1020)$ meson will play an important role in the study.

The above-mentioned effects of rescattering and regeneration in the hadronic phase is a subject of great interest. The heavy-ion collisions are used to study the QCD matter under extreme conditions of high temperatures and/or baryon densities with emphasis on the observation and study of the properties of the new state of matter–the so-called quark-gluon plasma (QGP). Once produced for a very short period of time, the QGP cannot be observed directly. Only simultaneous study of various theoretically predicted signatures of the QGP formation can be used for unambiguous results and conclusions. However, some of the signatures produced at the stage of the QGP are distorted and smeared out at

the later stages of the reactions. The hadronic gas produced at the later stages is known to distort the measured particle yields and p_T-shapes of their production spectra, the particle correlation and flow signals, the dilepton invariant mass spectra, etc. For this very reason, the models should be able to account for the later stages of the heavy-ion collisions to correctly interpret the experimental results. The short-lived resonances probe the properties of the hadronic phase and serve as a unique tool to study its properties. Properties of the resonances can be directly measured in the experiment and compared to the model predictions, thus validating the models and rejecting the wrong ones.

The properties of the hadronic phase are studied by measuring the ratios of resonance yields to yields of quasi-stable particles with similar quark contents such as $\rho(770)^0/\pi$, K*(892)/K, $\phi(1020)/K$, $\Lambda(1520)/\Lambda$, $\Sigma(1385)^{\pm}/\Lambda$ and $\Xi(1530)^0/\Xi$. The yield of quasi-stable particles is not significantly affected in the hadronic phase, while the measured yields of resonances are sensitive to the rescattering of daughter particles and regeneration of background hadrons. The resonances listed in Table 1 cover a wide range of lifetimes from ~1 fm/c for $\rho(770)^0$ to ~40 fm/c for $\phi(1020)$ mesons [10]. It makes these particles very useful to probe the hadronic phase properties. The combined effect of the hadronic phase depends on its lifetime and density (rescattering cross-sections).

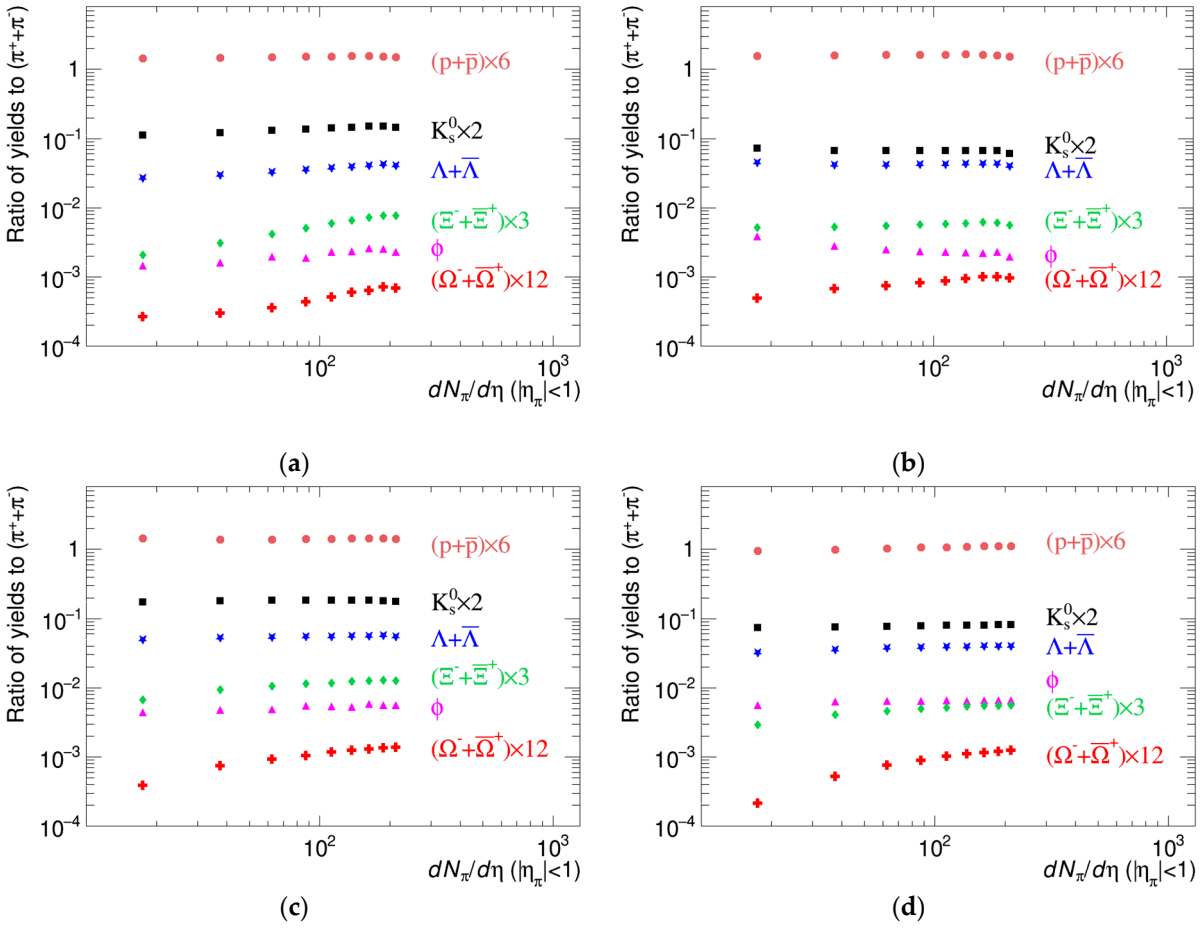

Figure 4. Ratios p/π, K^0_s/π, $\phi(1020)/\pi$, Λ/π, Ξ/π and Ω/π as a function of the final state charged particle multiplicity in Au + Au collisions at $\sqrt{s_{NN}}$ = 7.7 GeV as predicted by UrQMD [11] (**a**), AMPT [13] (**b**), PHSD [12] (**c**) and EPOS 1.99 [14] (**d**) event generators.

Figures 5 and 6 show the $\rho(770)^0/\pi$ and $K^*(892)^0/K$ ratios predicted by UrQMD [11], PHSD [12] and AMPT [13] event generators in Au + Au collisions at $\sqrt{s_{NN}}$ = 11 GeV. These event generators are used because they simulate the late hadronic cascades. The plots on the left show the $\rho(770)^0/\pi$ and $K^*(892)^0/K$ ratios as a function of the final state charged-

particle multiplicity, the ratios are normalized to unity in the most peripheral bin (start at one in the lowest-multiplicity interval). All event generators predict a suppressed production of $\rho(770)^0$ and $K^*(892)^0$ resonances in most central collisions, although the absolute values of suppression are quite different. The plots on the right show the double ratios, $(\rho(770)^0/\pi)_{\text{central}}/(\rho(770)^0/\pi)_{\text{peripheral}}$ and $(K^*(892)^0/K)_{\text{central}}/(K^*(892)^0/K)_{\text{peripheral}}$, as a function of the transverse particle momentum. The plots show that the suppression occurs at low momentum and that the particle ratios tend to unity at higher momenta. The suppression of the resonance yields in central heavy-ion collisions is explained by rescattering prevailing over regeneration for the shortest-lived resonances with $\tau < 20$ fm/c. Qualitatively similar suppression of $\rho(770)^0$ and $K^*(892)$ mesons was previously observed in heavy-ion collisions at RHIC and LHC energies [1,4,7]; the measurements were used to estimate the hadronic phase lifetime to be $\tau > 10$ fm/c in central Pb-Pb collisions at $\sqrt{s_{NN}}$ = 2.76 TeV [8]. Now a comparable suppression is predicted for the particles in heavy-ion collisions at NICA energies.

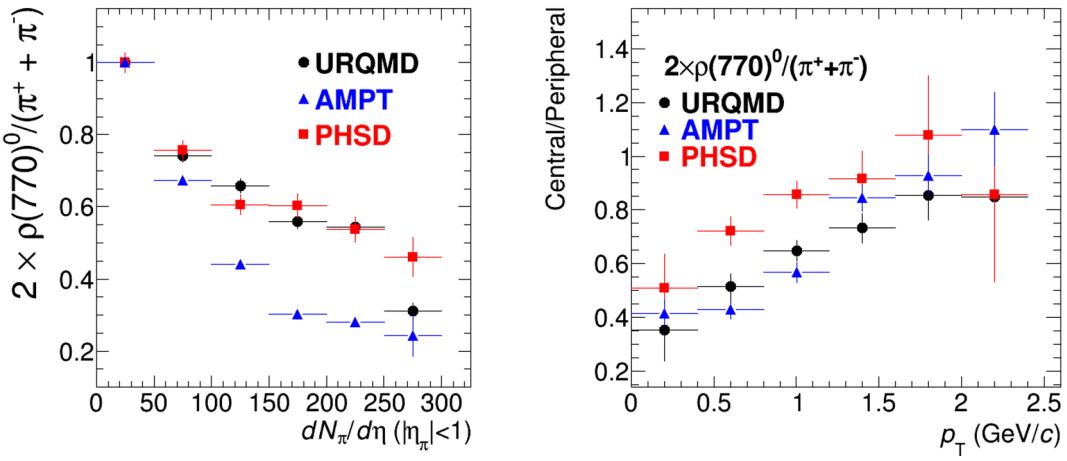

(**a**) (**b**)

Figure 5. Ratios $\rho(770)^0/\pi$ predicted by UrQMD [11], PHSD [12] and AMPT [13] event generators in Au + Au collisions at $\sqrt{s_{NN}}$ = 11 GeV. The $\rho(770)^0/\pi$ ratios normalized to unity in most peripheral collisions are shown as a function of the final state charged-particle multiplicity (**a**) and the $(\rho(770)^0/\pi)_{\text{central}}/(\rho(770)^0/\pi)_{\text{peripheral}}$ double ratio is shown as a function of the transverse particle momentum (**b**).

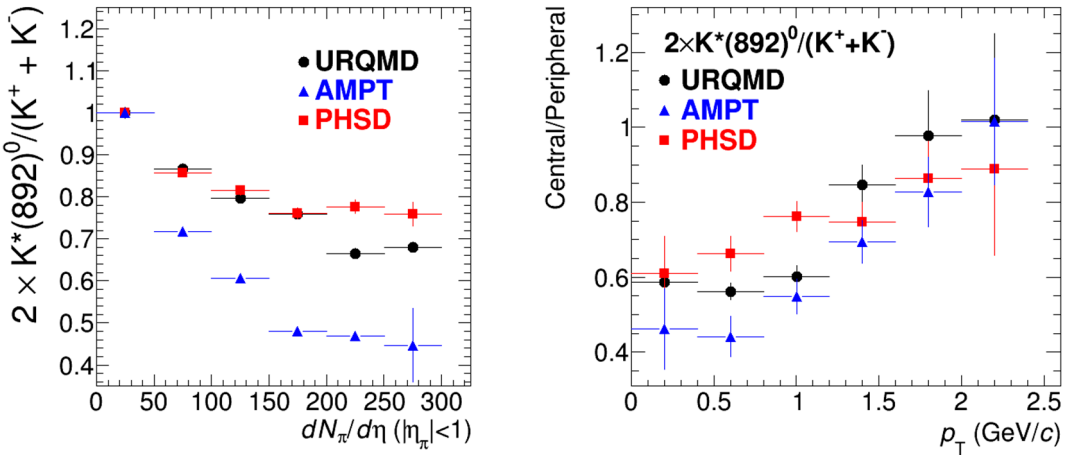

(**a**) (**b**)

Figure 6. Ratios $K^*(892)^0/K$ predicted by UrQMD [11], PHSD [12] and AMPT [13] event generators in Au + Au collisions at $\sqrt{s_{NN}}$ = 11 GeV. The K*(892)^0/K ratios normalized to unity in most peripheral collisions are shown as a function of the final state charged-particle multiplicity (**a**), and the $(K^*(892)^0/K)_{\text{central}}/(K^*(892)^0/K)_{\text{peripheral}}$ double ratio is shown as a function of the transverse particle momentum (**b**).

Figure 7 shows the ϕ(1020) /K ratio predicted by UrQMD [11], PHSD [12] and AMPT [13] event generators in Au + Au collisions at $\sqrt{s_{NN}}$ = 11 GeV. The plot on the left shows the ϕ(1020)/K ratio as a function of the final state charged-particle multiplicity. We observe a model-dependent ratio; the UrQMD and PHSD event generators predict the increasing ratio at higher multiplicities, while the AMPT generator predicts the decreasing ratio. At RHIC and LHC energies, the ratio showed a very weak dependence on multiplicity consistent with a flat ratio within uncertainties [2,4]. At NICA energies, the interplay between the rescattering and the regeneration depends on the model used to simulate the processes. The rescattering process for the longer-lived ϕ(1020) meson (τ~40 fm/c) is less important than that for $\rho(770)^0$ and K*(892) mesons (τ~1–5 fm/c) since only a small fraction of ϕ(1020) mesons decay in the hadronic phase while the importance of the regeneration effect does not depend on the resonance lifetime. The plot on the right shows the double ratio, $(\phi(1020)/K)_{central}/(\phi(1020)/K)_{peripheral}$, as a function of the transverse particle momentum. The plot confirms that the yield modifications for resonances occur at low momentum, where the effect of the hadronic phase is most prominent.

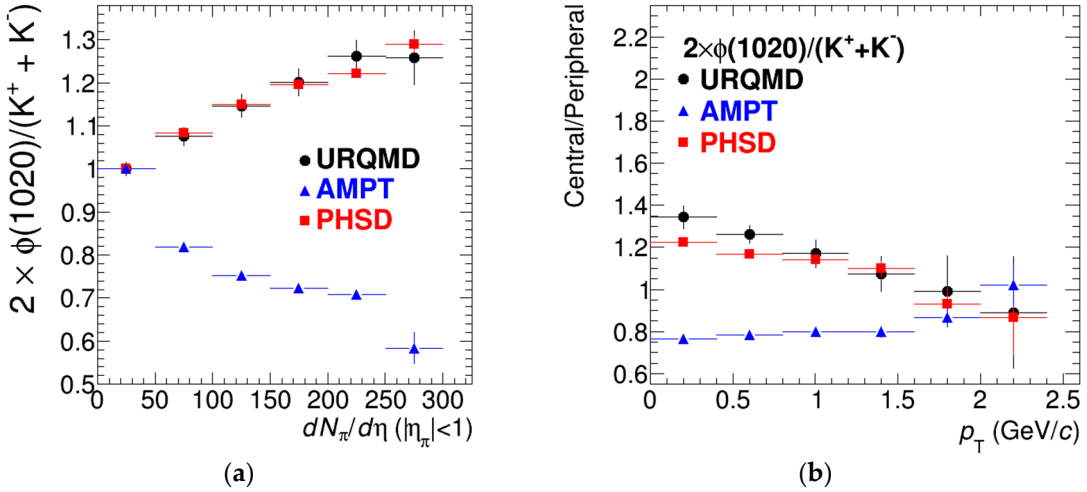

(**a**) (**b**)

Figure 7. Ratios ϕ(1020)/K predicted by UrQMD [11], PHSD [12] and AMPT [13] event generators in Au + Au collisions at $\sqrt{s_{NN}}$ = 11 GeV. The ϕ(1020)/K ratios normalized to unity in most peripheral collisions are shown as a function of the final state charged-particle multiplicity (**a**) and the $(\phi(1020)/K)_{central}/(\phi(1020)/K)_{peripheral}$ double ratio is shown as a function of the transverse particle momentum (**b**).

The rescattering and regeneration effects in the hadronic phase affect the final-state resonance properties in many aspects. Figure 1 shows that a significant part of the resonances produced at chemical freeze-out is not reconstructed in the hadronic decay channels due to the rescattering of daughter particles. Since the momentum distributions of the regenerating hadrons are exponential, the regeneration favors the production of lower-mass resonances. This can significantly distort the reconstructed line-shapes for resonances by lowering the mean masses and enhancing the lower mass tails in the invariant mass distributions. This effect is a subject of separate interest. Moreover, the effect should be taken into account when the particle yields are extracted from the invariant mass distributions using a given peak model, especially at low momentum. Another interesting feature that follows from Figure 1 is that the $\rho(770)^0$, ϕ(1020) and probably ω(892) resonance yields measured in the hadronic and dilepton decay channels should be quite different, the reconstructed yields in l^+l^- channels should be noticeably larger. The difference between the leptonic and hadronic decays is well captured in Figure 1. The resonances that are produced early in the system evolution and decay in the l^+l^- channel are not affected by the hadronic phase; the QCD matter is transparent for leptons. At the same time, a fraction of the hadronic decays is not reconstructed due to the rescattering of daughter particles. Actually, by disabling the resonance decays in Figure 1, we emulated the absence of rescattering

for l^+l^- decays. The regeneration effect plays the same role for the leptonic and hadronic decays. Qualitatively the difference of the $\rho(770)^0$ meson yields extracted in leptonic and hadronic decay channels can be even larger than that shown in Figure 1 since the effect of regeneration is underestimated when the $\rho(770)^0$ meson decays are disabled. Since about 30% of pions are produced from the $\rho(770)^0$ decays, the lower pion multiplicity due to disabled $\rho(770)^0 \to \pi^+\pi^-$ decays results in a smaller contribution of regeneration.

5. Conclusions

The reconstructed properties of the short-lived hadronic resonances predicted by UrQMD [11], PHSD [12], AMPT [13] and EPOS [14] general-purpose event generators are sensitive to the properties of the medium produced at different stages of the heavy-ion collisions at NICA energies. Among other things, the measurement of resonances will be used to study the properties of the hadronic phase and to tune the corresponding model calculations. An accurate description of the hadronic phase in the models is important for unambiguous interpretation of the experimental measurements for many observables such as the particle yields, correlations and collective flow coefficients.

Funding: This research was funded by RFBR according to the research project # 18-02-40038 and partially supported by the National Research Nuclear University MEPhI in the framework of the Russian Academic Excellence Project (contract No.02.a03.21.0005, 27.08.2013).

Institutional Review Board Statement: Not applicable.

Informed Consent Statement: Not applicable.

Data Availability Statement: Data available on request.

Conflicts of Interest: The funders had no role in the design of the study; in the collection, analyses, or interpretation of data; in the writing of the manuscript, or in the decision to publish the results.

References

1. Adams, J.; Aggarwal, M.M.; Ahammed, Z.; Amonett, J.; Anderson, B.D.; Arkhipkin, D.; Averichev, G.S.; Badyal, S.K.; Bai, Y.; Balewski, J.; et al. K(892)* resonance production in Au + Au and p + p collisions at $\sqrt{s_{NN}}$ = 200 GeV at STAR. *Phys. Rev. C* **2005**, *71*, 064902. [CrossRef]
2. Adler, S.S.; Afanasiev, S.; Aidala, C.; Ajitanand, N.N.; Akiba, Y.; Alexander, J.; Amirikas, R.; Aphecetche, L.; Aronson, S.H.; Averbeck, R.; et al. Production of ϕ mesons at midrapidity in $\sqrt{s_{NN}}$ = 200 GeV Au + Au collisions at relativistic energies. *Phys. Rev. C* **2005**, *72*, 014903. [CrossRef]
3. Abelev, B.; Aggarwal, M.M.; Ahammed, Z.; Amonett, J.; Anderson, B.D.; Anderson, M.; Arkhipkin, D.; Averichev, G.S.; Bai, Y.; Balewski, J.; et al. Strange Baryon Resonance Production in $\sqrt{s_{NN}}$ = 200 GeV p + p and Au + Au collisions. *Phys. Rev. Lett.* **2006**, *97*, 132301. [CrossRef] [PubMed]
4. Abelev, B.; Adam, J.; Adamová, D.; Aggarwal, M.M.; Agnello, M.; Agostinelli, A.; Agrawal, N.; Ahammed, Z.; Ahmad, N.; Masoodi, A.A.; et al. [ALICE Collaboration] K*(892)^0 and ϕ(1020) production in Pb-Pb collisions at $\sqrt{s_{NN}}$ = 2.76 TeV. *Phys. Rev. C* **2015**, *91*, 024609. [CrossRef]
5. Adamová, D.; ALICE Collaboration; Aggarwal, M.M.; Rinella, G.A.; Agnello, M.; Agrawal, N.; Ahammed, Z.; Ahmad, S.; Ahn, S.U.; Aiola, S.; et al. Production of $\Sigma(1385)^{\pm}$ and $\Xi(1530)^0$ in p-Pb collisions at $\sqrt{s_{NN}}$ = 5.02 TeV. *Eur. Phys. J. C* **2017**, *77*, 389. [CrossRef]
6. Acharya, S.; Adamová, D.; Adolfsson, J.; Aggarwal, M.M.; Rinella, G.A.; Agnello, M.; Agrawal, N.; Ahammed, Z.; Ahn, S.U.; Aiola, S.; et al. Suppression of $\Lambda(1520)$ resonance production in central Pb-Pb collisions at $\sqrt{s_{NN}}$ = 2.76 TeV. *Phys. Rev. C* **2019**, *99*, 024905. [CrossRef]
7. Acharya, S.; Acosta, F.T.; Adamová, D.; Adolfsson, J.; Aggarwal, M.M.; Rinella, G.A.; Agnello, M.; Agrawal, N.; Ahammed, Z.; Ahn, S.U.; et al. Production of the ρ(770)0 meson in pp and Pb-Pb collisions at $\sqrt{s_{NN}}$ = 2.76 TeV. *Phys. Rev. C* **2019**, *99*, 064901. [CrossRef]
8. Acharya, S.; Adamová, D.; Adler, A.; Adolfsson, J.; Aggarwal, M.; Rinella, G.A.; Agnello, M.; Agrawal, N.; Ahammed, Z.; Ahmad, S.; et al. Evidence of rescattering effect in Pb–Pb collisions at the LHC through production of K(892)0* and ϕ(1020) mesons. *Phys. Lett. B* **2020**, *802*, 135225. [CrossRef]
9. Blaschke, D.; Aichelin, J.; Bratkovskaya, E.; Friese, V.; Gazdzicki, M.; Randrup, J.; Rogachevsky, O.; Teryaev, O.; Toneev, V. Topical issue on Exploring Strongly Interacting Matter at High Densities-NICA White Paper. *Eur. Phys. J. A* **2016**, *52*, 267. [CrossRef]
10. Particle Data Group; Zyla, P.A.; Barnett, R.M.; Beringer, J.; Dahl, O.; Dwyer, D.A.; Groom, D.E.; Lin, C.-J.; Lugovsky, K.S.; Pianori, E.; et al. Review of Particle Physics. *Prog. Theor. Exp. Phys.* **2020**, *2020*, 083C01. [CrossRef]
11. Bass, S.A. Microscopic models for ultrarelativistic heavy ion collisions. *Prog. Part. Nucl. Phys.* **1998**, *41*, 255–369. [CrossRef]

12. Bratkovskaya, E.L.; Cassing, W.; Moreau, P.; Oliva, L.; Soloveva, O.E.; Song, T. PHSD—A Microscopic Transport Approach for Strongly Interacting Systems. *arXiv Prepr.* **2019**, arXiv:1908.00451.
13. Lin, Z.; Ko, C.M.; Li, B.-A.; Zhang, B.; Pal, S. Multiphase transport model for relativistic heavy ion collisions. *Phys. Rev. C* **2005**, *72*, 064901. [CrossRef]
14. Pierog, T.; Karpenko, I.A.; Katzy, J.M.; Yatsenko, E.; Werner, K. EPOS LHC: Test of collective hadronization with data measured at the CERN Large Hadron Collider. *Phys. Rev. C* **2015**, *92*, 034906. [CrossRef]
15. Baznat, M.; Botvina, A.; Musulmanbekov, G.; Toneev, V.; Zhezher, V. Monte-Carlo Generator of Heavy Ion Collisions DCM-SMM. *Phys. Part. Nucl. Lett.* **2020**, *17*, 303–324. [CrossRef]
16. Vislavicius, V.; Kalweit, A. Multiplicity dependence of light flavour hadron production at LHC energies in the strangeness canonical suppression picture. *arXiv Prepr.* **2016**, arXiv:1610.03001.
17. ALICE Collaboration. Enhanced production of multi-strange hadrons in high-multiplicity proton–proton collisions. *Nat. Phys.* **2017**, *13*, 535–539. [CrossRef]